UDK 621.315.592

Design of tunnel-coupled quantum wells for a Mach–Zehnder scheme modulator construction

© A.I. Bobrov[1], N.V. Baidus'[1], S.V. Khazanova[2], A.P. Gorshkov[2], K.V. Sidorenko[1], A.N. Shushunov[1], N.V. Malekhonova[1], A.V. Nezhdanov[2], A.V. Zdoroveyshchev[1], V.N. Trushin[1], E.V. Ubyivovk[3], A.I. Okhapkin[4], D.S. Klement'ev[2], Z.Sh. Gasainiev[5], A.V. Kharlamov[6]

[1] Research Institute for Physics and Technology, Lobachevsky State University of Nizhny Novgorod, 603022 Nizhny Novgorod, Russia
[2] Lobachevsky State University, 603022 Nizhny Novgorod, Russia
[3] St. Petersburg State University, 199034 St. Petersburg, Russia
[4] Institute of Physics of Microstructures, Russian Academy of Sciences, 603950 Nizhny Novgorod, Russia
[5] Scientific-Production Enterprise Salyut JSC", 603950 Nizhny Novgorod, Russia
[6] „T8" LLC, 107076 Moscow, Russia

E-mail: khazanova@phys.unn.ru

Received June 18, 2022
Revised June 25, 2022
Accepted June 25, 2022

In this paper, we propose a method for predicting the refractive index variation in InGaAlAs tunnel-coupled quantum wells under the action of an electric field. Complex of mathematical and experimental studies to optimize the heterosystems design forthe semiconductor modulator construction according to a planar Mach–Zehnder interferometer scheme is demonstrated.

Keywords: Mach–Zehnder modulator, nanoheterostructure, quantum mechanical calculations, refractive index, transmission electron microscopy, photoelectric spectroscopy.

DOI: 10.21883/SC.2022.09.54123.35

1. Introduction

Planar Mach–Zehnder modulators are used widely to transmit data in modern fiber-optic networks. They find application in telecommunications [1], radio detecting and ranging [2], and optical signal microprocessors [3].

Their operation is based on control over the conditions of interference of laser radiation, which is split by a system of waveguides into two coherent wave fronts, within a microoptical circuit designed as a planar Mach–Zehnder interferometer. The modulation effect is achieved due to the influence of the electric component of a microwave electromagnetic wave on the refraction index of a medium within which laser radiation is propagating [4].

Planar Mach–Zehnder modulators based on lithium niobate are commonly applied in the construction of backbone fiber telecommunications lines. Their dimensions are relatively large, with lengths reaching 50 mm. This is attributable to the fact that the strength of variation of the refraction index under the influence of an electric field in lithium niobate is limited, and the limits are set by the crystal structure of this ferroelectric material [5]. The indicated dimensions make such devices suited mostly for specialized applications [6].

A modular may be made more compact by substituting lithium niobate with periods of heteronanostructures based on group $A^{III}B^{V}$ semiconductors. This allows one to design devices as small as 3 mm in length [6,7].

The needed variation of the refraction index under the influence of an electric is achieved due to the quantum-confined Stark effect in strained tunnel-coupled quantum wells (TCQWs) [8–11].

A number of research groups are currently working on optimization of the TCQW design for enhancing the performance of semiconductor planar Mach–Zehnder modulators [2,12,13].

It should be noted that the Stark effect in an isolated quantum well is fairly weak. Heteronanostructures consisting of several tunnel-coupled QWs are needed to raise the modulation efficiency [9].

Thus, the key objective in engineering a semiconductor planar Mach–Zehnder modulator is to determine the optimum TCQW design that provides the strongest variation of the refraction index at optical wavelengths within the C-band of transparency of quartz fiber ($\lambda \sim 1530-1565$ nm). The preservation of fine frequency characteristics of state switching, which are also governed

by the heterostructure parameters, is a prerequisite for the design of a fast heterostructure-based modulator [9].

In view of the complexity and time intensiveness of fabrication of quantum-dimensional structures, it is crucial to provide a means for predictive modeling of the heterostructure design via mathematical simulation.

That said, reliable predictions regarding the characteristics of structures with strained tunnel-coupled quantum wells cannot be made without calibration of the results of theoretical calculations against experimental data obtained using structural monitoring methods. Data on the distribution of components of a solid solution in the crystal lattice of epitaxial layers are important in this regard [14]. These data acquire practical utility in combination with the results of measurements of the optical properties of the studied heterosystem, thus making it possible to identify the relation between structural and energetic parameters of tunnel-coupled quantum wells [15].

A combination of cross-section high-resolution transmission electron microscopy (HR TEM) and X-ray diffraction analysis was used to examine the structure. The optical properties of the objects under study were determined by measuring the photocurrent.

The importance of the present study stems from the fact that it combines objective monitoring with numerical calculations of the energy band diagram, envelopes of wave functions, and the associated optical characteristics.

The proposed methodologies should help raise the predictive validity of mathematical simulations of systems with tunnel-coupled quantum wells and thus speed up the advancements in design of semiconductor planar Mach–Zehnder modulators.

2. Studied structures

A group of asymmetric $In_xGa_{1-x}As/Al_xGa_{1-x}As/In_xGa_{1-x}As$ TCQWs (Fig. 1) in the intrinsic conductivity region of a $p-i-n$ diode was chosen as an example to demonstrate the proposed method. A detailed description of the structure is given in Table 1.

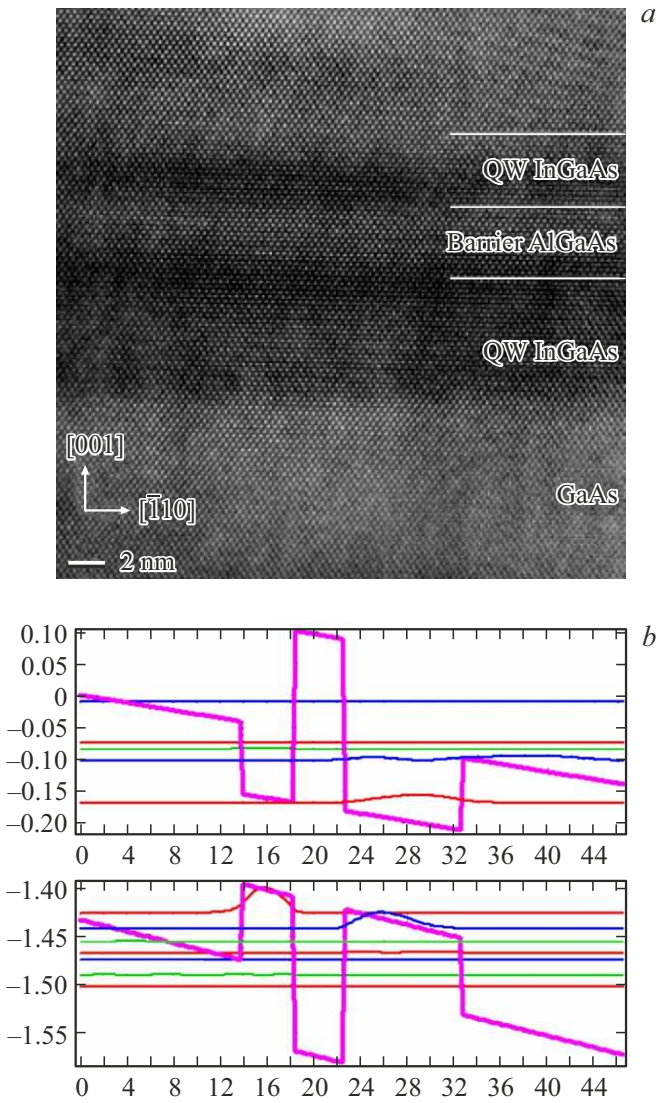

Figure 1. *a* — HR TEM image of the studied structure with $GaAs/In_xGa_{1-x}As/Al_xGa_{1-x}As/In_xGa_{1-x}As/GaAs$ TCQWs. *b* — calculated potential profile of the $GaAs/In_xGa_{1-x}As/Al_xGa_{1-x}As/In_xGa_{1-x}As/GaAs$ structure and energy spectrum. (A color version of the figure is provided in the online version of the paper.

Table 1. Specifics of the design of the studied heteronanostructure

Layer thickness, nm	Description	
Substrate	GaAs	$n^+ = 10^{18}$ cm^{-3}
500	GaAs	$n^+ = 10^{18}$ cm^{-3}
200	GaAs	$n = 10^{16}$ cm^{-3}
50	GaAs	$n = 10^{16}$ cm^{-3}
9.5	$In_xGa_{1-x}As$	$x = 0.19$
4	$Al_xGa_{1-x}As$	$x = 0.2$
4	$In_xGa_{1-x}As$	$x = 0.19$
50	GaAs	$p = 10^{16}$ cm^{-3}
200	GaAs	$p = 10^{16}$ cm^{-3}
300	GaAs	$p^+ = 10^{18}$ cm^{-3}

The structure was fabricated by MOS hydride epitaxy using an AIX200RF (Aixtron, Germany) setup.

The specific type of a heteronanostructure was chosen based on the data reported in [16–20], where the variation of the refraction index in a system of asymmetric double tunnel-coupled QWs (AD-TCQWs) in an electric field was demonstrated to be significantly more pronounced than the corresponding variation in single or double symmetric QWs. This is attributable to the effects of redistribution of the electron density in adjacent quantum wells and variation of the probability of interband transitions with exciton contributions included; the net result is that the quantum Stark effect is amplified.

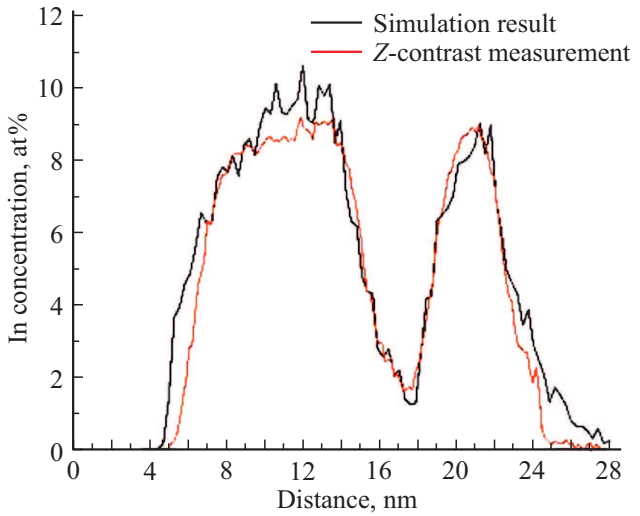

Figure 2. Concentration profile of indium in the structure measured using a combination of transmission electron microscopy techniques. The concentration of indium (in at%) is related to parameter x in the chemical formula of solid solution $In_xGa_{1-x}As$ in a ratio of 2 : 1.

The structure of the object under study was examined with a Libra 200FE (Zeiss, Germany) transmission electron microscope. Profiling of the elemental composition was performed using a combination of the Z-contrast method and energy-dispersive X-ray spectroscopy. Equipment provided by the „Nanotechnologies“ resource center (Research Park, St. Petersburg University) was used in these experiments.

The HR TEM data were calibrated against the results of examination with a D8 DISCOVER (Bruker, Germany) high-resolution X-ray diffractometer and a DIFFRAC plus LEPTOS 7 software suite that is used to analyze X-ray diffraction patterns and calculate the parameters of heteronanostructures based on them. The error of determination of the indium concentration in $In_xGa_{1-x}As$ layers was $\leq 5\%$ (Fig. 1, *a*).

The elemental composition profile measured using a combination of transmission electron microscopy techniques was compared with the results of numerical simulation of the growth process carried out with account for In segregation in accordance with the algorithm detailed in [21]. The model was found to agree qualitatively and quantitatively with the experiment (Fig. 2).

The composition profile was updated to match the experimental data and used to perform numerical simulation of the energy bands and calculate size quantization levels, envelopes of wave functions, and matrix elements of interband transitions of the studied structure.

The photoabsorption edges (Fig. 3) were calculated in a similar fashion. The obtained data were verified via photocurrent spectroscopy for the $p-i-n$ diode (Fig. 4).

The quantum-confined Stark effect was analyzed by measuring the spectral dependences of photocurrent at a temperature of 300 K. An MDR-2 monochromator with a 100 W halogen lamp served as the source of monochromatic radiation. Measurements were performed with a variable signal; a Stanford Research Systems SR540 mechanical optical modulator operating at a frequency of 130 Hz was used for this purpose. The variable electric signal was detected using the standard „lock-in“ procedure with a Stanford Research Systems SR510 selective amplifier. A spectral dependence of the relative photosensitivity was plotted based on the results of examination of photoelectric spectra:

$$S_{ph}(\hbar\omega) = I_{ph}(\hbar\omega)/L(\hbar\omega), \quad (1)$$

where $I_{ph}(\hbar\omega)$ is the photocurrent and $L(\hbar\omega)$ is the irradiation intensity in arbitrary units.

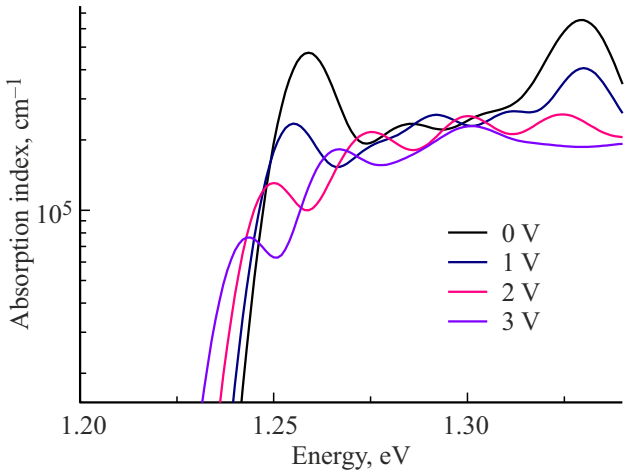

Figure 3. Absorption spectra of the studied structure obtained via mathematical simulation at different voltages applied to quantum wells in the transverse direction.

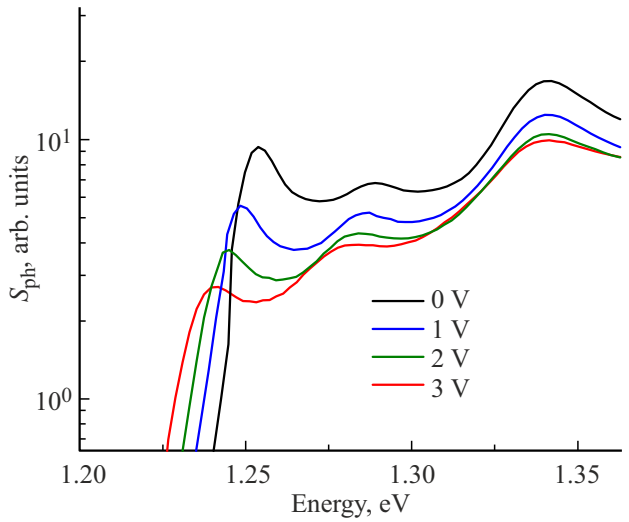

Figure 4. Spectral dependences of the photocurrent in the interband absorption region of a double TCQW measured at different reverse bias values at the $p-i-n$ diode.

3. Simulation and calculation procedure

The self-consistent solution of Schrödinger and Poisson equations in the effective mass approximation was used to calculate the profiles of energy bands, size quantization levels, and envelopes of wave functions in a TCQW system in a transverse electric field. A numerical approach based on the finite difference method was used to solve these equations. Calculations were performed in the Lazarus software package.

The actual concentration profile of indium in the heterostructure, which was determined using a combination of transmission electron microscopy and X-ray diffraction analysis, was factored into these calculations. The calculation procedure was detailed in [15]. The matrix elements of interband transitions in TCQWs were calculated based on the numerical simulation data.

The above algorithm was used to examine the redistribution of electron density in TCQW systems due to the quantum-confined Stark effect. The results of model calculations were used to determine the redshift of absorption spectra caused by the rearrangement of interband and exciton transitions in stronger electric fields applied in the direction of structure growth.

The theoretical approach to analyzing the influence of an applied transverse electric field on the variation of refraction index of the heterostructure is detailed below.

It is known that optical absorption coefficient $\alpha(\hbar\omega)$ is related to the imaginary part of permittivity in the following way:

$$\alpha(\hbar\omega) = \frac{\omega}{cn}\,\varepsilon(\hbar\omega), \tag{2}$$

where c is the speed of light and n is the refraction index of the material.

Interband absorption is governed by the transitions between size quantization levels of electrons and (heavy) holes. The probability of such a transition is calculated based on the overlap integral of wave functions of an electron and a hole. In addition, an exciton peak in the absorption spectrum is produced due to the Coulomb interaction of an electron and a hole. Therefore, the absorption spectrum is shaped by interband and exciton contributions and depends on the binding energy and the radius of an exciton.

Let us present the imaginary part of permittivity as a sum of interband and exciton transitions:

$$\varepsilon(\hbar\omega) = \varepsilon^{\text{band}}(\hbar\omega) + \varepsilon^{\text{ex}}(\hbar\omega). \tag{3}$$

The contribution of interband transitions to permittivity is [8]

$$\varepsilon^{\text{band}}(\hbar\omega) = \frac{e^2}{\varepsilon_0 m_0^2 \omega^2 L_z}\,\frac{m_{eh}}{\pi\hbar^2}\sum_{i,j}|M_b|^2|M_{ij}|^2 \times \int_0^\infty G\cdot\Gamma(\Delta E_g + E_{ei} + E_{hj} - \hbar\omega)dE, \tag{4}$$

L_z — is the QW width; m_{eh} is the reduced effective mass of a hole and an electron; e is the electron charge; E_{ei}, E_{hj} are size quantization levels of an electron and a hole, respectively; E_g is the band gap; and $|M_b|^2$ is the matrix element of Bloch states, which is defined as [22]

$$|M_b|^2 = \frac{m_0^2 E_g(E_g+\Delta)}{12m_e(E_g+\frac{2}{3}\Delta)}, \tag{5}$$

where m_e is the effective electron mass and Δ is the spin-orbit splitting energy.

$$|M_{ij}|^2 = \left|\int \psi_{el}(z)\psi_{hj}(z)dz\right|^2$$

— is the overlap integral of envelopes of wave functions of an electron and a hole and G is the matrix element that depends on polarization of incident light. This factor for light with its polarization parallel to the heterostructure plane (TE mode) assumes a value of 3/2 for heavy hole–electron and transitions and 1/2 for light hole–electron transitions [8]. Γ is the spectral line profile, which is Gaussian in the present case:

$$\Gamma(x) = \frac{1}{\sigma\sqrt{\pi}}\,e^{x^2/(\sigma\sigma)}, \tag{6}$$

where σ is a parameter specifying the HWHM of a line.

The exciton contribution to permittivity is [8]

$$\varepsilon^{\text{ex}}(\hbar\omega) = \frac{2\pi e^2}{\pi\varepsilon_0 m_0^2\cdot L_z\omega^2} \times |M|^2|M_{ij}|^2|\varphi_{\text{ex}}(0)|^2 G\Gamma(E_{\text{ex}}-\hbar\omega), \tag{7}$$

E_{ex} — is the exciton energy, $\varphi_{\text{ex}}(0) = \alpha\sqrt{2/\pi}$ — is the wave function of a two-dimensional exciton, and α is a variational parameter corresponding to the reciprocal Bohr radius of an exciton. The binding energy and the Bohr radius of an exciton were calculated in accordance with a variational procedure detailed in [23].

If the variation of the absorption spectrum of a sufficiently wide spectral region is known, the Kramers–Kronig relations may be used to determine the variation of the refraction index spectrum under the influence of an applied electric field [24]:

$$\Delta n(\hbar\omega) = \frac{c\hbar}{\pi}\,P\int_{\hbar\omega 1}^{\hbar\omega 2}\frac{\Delta\alpha(\hbar\omega')}{(\hbar\omega')^2-(\hbar\omega)^2}\,d(\hbar\omega'), \tag{8}$$

where $(\hbar\omega 1, \hbar\omega 2)$ is the energy range and symbol P indicates that the integral is a principal-value one. The parameters of the $In_xGa_{1-x}As/Al_xGa_{1-x}As/In_xGa_{1-x}As$ heterostructure used in calculation of its optical properties are listed in Table 2.

Table 2. Parameters of the $In_xGa_{1-x}As/Al_xGa_{1-x}As/In_xGa_{1-x}As$ structure used in calculations

Band gap of $Al_xGa_{1-x}As$, E_g, eV	$1.424 + 1.247x$
Effective electron mass in $Al_xGa_{1-x}As$, m_e	$0.0665 + 0.0835x$
Effective heavy hole mass in $Al_xGa_{1-x}As$, m_h	$0.34 + 0.42x$
Band gap of $In_xGa_{1-x}As$, E_g, eV	$1.424 - 1.615x + 0.555x^2$
Effective electron mass in $In_xGa_{1-x}As$, m_e	$0.0665 - 0.05x + 0.0065x^2$
Effective heavy hole mass in $In_xGa_{1-x}As$, m_h	$0.34 + 0.794x$
Spin-orbit splitting energy, Δ, eV	0.33
HWHM of the spectral line profile, δ, eV	0.011

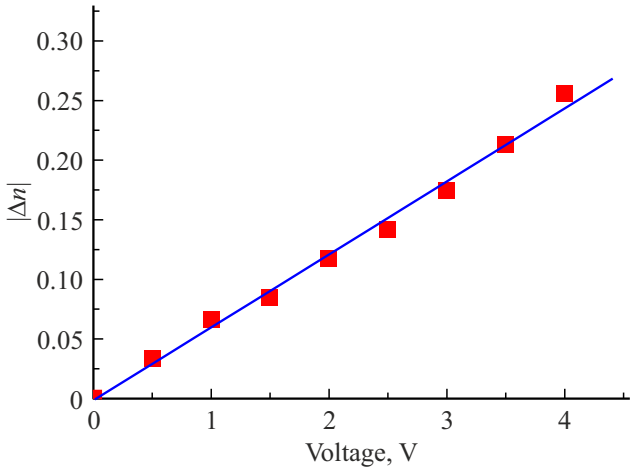

Figure 5. Magnitude of the refraction index variation under different control voltages applied to the structure.

4. Results and discussion

The optical absorption spectra of a system of asymmetric double TCQWs were calculated with the exciton contribution factored in (Fig. 3). The obtained results demonstrate that a noticeable redistribution of the electron density occurs in a system of quantum wells when the electric field strength increases. This translates into a redshift of the optical spectrum due to the quantum-confined Stark effect. It was demonstrated that the chosen structure features a $\sim 10-15$ meV redshift of the exciton absorption peak corresponding to a variation of the electric field applied in the direction of structure growth within the 0–3 V range. The photocurrent measurement data verify this result (Fig. 4).

Spectra of the refraction index variation $\Delta n(\hbar\omega)$ with bias voltage were obtained using the Kramers–Kronig relations and the absorption index values calculated in a wide spectral region [24]. Figure 5 demonstrates the variation of the refraction index magnitude for the studied structure under the influence of an electric field at wavelength $\lambda = 1550$ nm.

5. Conclusion

Thus, the feasibility of application of a combination of mathematical simulation, growth experiment, and objective monitoring of the physical parameters of heteronanostructures for predicting the optical properties of strained tunnel-coupled quantum wells and optimizing their design with the purpose of constructing efficient planar Mach–Zehnder modulators was demonstrated. Subsequent studies will be aimed at verifying experimentally the calculated values of the refraction index variation under the influence of an electric field.

Funding

This study was performed as part of the „Priority 2030“ academic leadership program, No. N-423-99_2022-2022.

Conflict of interest

The authors declare that they have no conflict of interest.

References

[1] Ke Liu, Chen Ran Ye, Sikandar Khan, Volker J. Sorger. Laser Photon. Rev., **9** (2), 172 (2015).
[2] Y. Miyazeki, T. Arakawa. Jpn. J. Appl. Phys., **58**, SJJE05 (2019).
[3] Chong Li, Xiang Zhang, Jingwei Li, Tao Fang, Xiaowen Dong. Photonix, **2**, 20 (2021).
[4] R.G. Walker, J. Lightw. Technol., **5** (10), 1444 (1987).
[5] E.L. Wooten, Karl M. Kissa, Alfredo Yi-Yan, Edmond J. Murphy, Senior Member, Donald A. Lafaw, Peter F. Hallemeier, David Maack, Daniel V. Attanasio, Daniel J. Fritz, Gregory J. McBrien, Donald E. Bossi. IEEE J. Select. Top. Quant. Electron., **6** (1), 69 (2000).
[6] R.G. Walker, Yi Zhou. Frontiers Phys., **9**, 636002 (2021).
[7] K. Tsuzuki, T. Ishibashi, T. Ito, S. Oku, Y. Shibata, T. Ito, R. Iga, Y. Kondo, Y. Tohmori. IEEE Photon. Technol. Lett., **17** (1), 46 (2005).
[8] Kenji Nakamura, Akira Shimizu, Kazuhito Fujii, Masanori Koshiba, Senior Member, Kazuya Hayata. IEEE J. Quant. Electron., **28** (7), 1670 (1992).
[9] Hao Feng, J.P. Pang, M. Sugiyama, Kunio Tada, Yoshiaki Nakano. IEEE J. Quant. Electron., **34** (7), 1197 (1998).
[10] Zhixin Xu. Proc. SPIE, **7135**, 71350Y-1 (2008).
[11] V.V. Zolotarev, I.S. Shashkin,V.S. Golovin, O.S. Soboleva, V.V. Shamakhov, S.O. Slipchenko, N.A. Pikhtin. Semicond. Sci. Technol., **34**, 095005 (2019).
[12] M. Stepanenko, I. Yunusov, V. Arykov, P. Troyan, Yu. Zhidik. Symmetry, **12** (11), 1920 (2020).

[13] Guang Qian, Bin Niu, Wu Zhao, Qiang Kan, Xiaowen Gu, Fengjie Zhou, YuechanKong, Tangsheng Chen. Chinese Optics Lett., **17** (6), 061301 (2019).
[14] C. Kittel. Quantum Theory of Solids (N.Y., John Wiley and Sons, 1963).
[15] S.V. Khazanova, V.E. Degtyarev, N.V. Malekhonova, D.A. Pavlov, N.V. Baidus. Semiconductors, **49** (1), 55 (2015).
[16] M.K. Chin. J. Appl. Phys., **76**, 518 (1994).
[17] N. Susa. J. Appl. Phys., **73**, 932 (1993).
[18] Yasunori Tokuda, Kyozo Kanamoto, Yuji Abe, Noriaki Tsukada. Phys. Rev. B, **41**, 10280 (1990).
[19] C. Thirstrup. IEEE J. Quant. Electron., **31**, 988 (1995).
[20] P. Steinmann, B. Borchert, B. Stegmuller. IEEE Photon. Technol. Lett., **9**, 191 (1997).
[21] S.V. Khazanova, M.I. Vasilevskiy. Semicond. Sci. Technol., **25**, 085008 (2010).
[22] H.C. Casey, M.B. Panish. Heterostructure Lasers, Part A (N.Y., Academic, 1978) chap. 3.6, p. 146.
[23] D.A.B. Miller, D.S. Chemla, T.S. Damen, C. Gossard, W. Wiegmann, T.H. Wood, C.A. Burrus. Phys. Rev. B, **32** (2), 1043 (1985).
[24] R. de L. Kronig. J. Opt. Soc. Am., **12** (6), 547 (1926).